Generation of Coastal Inertial Oscillations by Time-Varying Wind

PIJUSH K. KUNDU

Nova University, Oceanographic Center, Dania, FL 33004

(Manuscript received 25 June 1984, in final form 19 September 1984)

ABSTRACT

The excitation of coastal inertial oscillations by a rapidly varying wind is investigated. It is shown that the mean-square response to a completely random forcing is $\overline{\psi^2} \propto \int \psi_\delta^2 dt$, where ψ_δ is the response to impulsive forcing and the integral is over the record length. The rms response therefore initially increases with time as $t^{1/2}$, and reaches stationarity in the decay scale for ψ_δ. As in the random-walk problem, the $t^{1/2}$ increase is a result of the superposition of uncorrelated steps. Continuous random forcing preferentially increases subsurface amplitudes, since the energy flux from the coast–surface corner causes a surface decay and a subsurface growth of ψ_δ.

With assumed parameters, a step-input wind forcing of 1 dyn cm^{-2} generates inertial oscillations of 4 cm s^{-1} in the surface layer and 0.7–1.5 cm s^{-1} below. With a random wind in the range (−0.5, 0.5) dyn cm^{-2}, the surface values increase to 8–11 cm s^{-1} and the subsurface values to 3–7 cm s^{-1}. With an observed wind-forcing the surface and subsurface amplitudes are 10–17 cm s^{-1} and 5–9 cm s^{-1}, respectively. Compared to the step-input wind, the oscillations due to a randomly varying wind are less coherent in the vertical and more intermittent in time.

1. Introduction

The inertial oscillations observed in the surface layer can generally be explained by the wind forcing (Pollard and Millard, 1970). The source of subsurface inertial oscillations, on the other hand, has been the subject of some controversy. Pollard (1970) studied an open-ocean model forced by the sudden application of a constant wind stress (that is, a step input), in which the spatial dependence of the wind stress resulted in the vertical and horizontal dispersion of the inertial energy. He found, however, that a wind stress of 1 dyn cm^{-2} resulted in a maximum amplitude just below the mixed layer of only about 1 cm s^{-1}; farther below, the amplitude decayed sharply to negligible values. Only wind stresses of hurricane magnitude (Price, 1983; Gill, 1984) can therefore explain the observed magnitudes of inertial oscillations (10–20 cm s^{-1}) within and above the thermocline. Below the thermocline, mechanisms other than wind stresses have been suggested to dominate.

Kundu *et al.* (1983, henceforth referred to as KCM) studied a coastal model and forced it with an alongshore wind in the form of the customary step input. The forcing was assumed spatially uniform, but the spatial inhomogeneity necessary for vertical dispersion resulted from the presence of the coast. Since the inertial oscillations are circularly polarized, the vanishing normal-velocity condition resulted in a rapid decay of the oscillations near the coast (coastal inhibition), forcing a *downward flux of inertial energy from the surface–coast corner.* As found by Pollard (1970), however, the maximum subsurface amplitude was much lower than observed—less than 1 cm s^{-1} for a 1 dyn cm^{-2} wind.

The KCM calculations cannot therefore explain the large subsurface inertial oscillations observed in coastal regions (Kundu, 1976b; Thomson and Huggett, 1981; Denbo and Allen, 1984; Hamilton, 1984). For example, maximum subsurface amplitudes of 10–13 cm s^{-1} have been observed near the coast of Oregon during a period in which the wind was less than 4 dyn cm^{-2}. Compared to the observations, the KCM model oscillations are also too highly correlated in the vertical, and not intermittent enough in time.

It was subsequently suggested (Kundu, 1984) that one possible way to increase the subsurface amplitudes, without proportionally increasing the surface amplitudes, might be a rapidly varying forcing with time scales less than an inertial period. Fluxes of inertial energy would be constantly pumped downward from the coast–surface corner with every change of the wind. Their random superposition is expected to generate the large subsurface amplitudes, high intermittency, and low vertical coherence.

The generation of inertial oscillations due to a time-varying wind forcing will be studied in this paper. In particular, we shall investigate whether a time varying wind generates subsurface oscillations that are realistic, that are large enough in magnitude, sufficiently intermittent in time, and have small enough coherence scale in the vertical. It will be found that the random wind application greatly improves the KCM model results.

Before presenting the coastal solutions due to a rapidly varying wind, some general relationships between the forcing and the response are developed in the next section.

2. Considerations of time varying wind

For linear systems, the response $\psi(t)$ due to a time varying forcing $\tau(t)$ can be obtained by superposing solutions $\psi_H(t)$ due to a unit Heaviside step forcing $\tau = H(t)$. To be specific, $\tau(t)$ may be the wind stress and $\psi(t)$ may be any resulting flow variable such as pressure or a velocity component. The variables ψ and ψ_H may also depend on location $\mathbf{x}$, but this dependence will be suppressed for notational simplicity.

The linear superposition leads to the convolution integrals

$$\psi(t) = \int_{-0}^{t} \frac{d\tau}{d\alpha}\,\psi_H(t-\alpha)d\alpha = \int_0^t \tau(\alpha)\,\frac{d\psi_H}{dt}\,(t-\alpha)d\alpha. \tag{1}$$

It is assumed that $\tau = 0$ for $t < 0$. However, the lower limit (-0) in the first integral covers the case in which τ has a discontinuity at $t = 0$. It is evident that $d\psi_H/dt$ is Green's function for the system, that is, the response to a delta function forcing. One usually calls $\psi_\delta \equiv d\psi_H/dt$ the impulse response, as opposed to the step response ψ_H.

The linear superposition of solutions results in a general spectral relationship between the forcing and the response. Let $\hat{\ }$ denote the finite Fourier transform for a record length T. Equation (1) then gives

$$\hat{\psi} = \hat{\psi}_\delta \hat{\tau}. \tag{2}$$

The response and forcing spectra are respectively defined as

$$S_\psi(\omega) = \lim_{T\to\infty}\left(\frac{\hat{\psi}\hat{\psi}\dagger}{T}\right); \quad S_\tau(\omega) = \lim_{T\to\infty}\left(\frac{\hat{\tau}\hat{\tau}\dagger}{T}\right),$$

where $(\ )\dagger$ denotes complex conjugation. Equation (2) therefore gives

$$S_\psi = |\hat{\psi}_\delta|^2 S_\tau, \tag{3}$$

which relates the response spectrum S_ψ to the forcing spectrum S_τ by means of the transfer function $\hat{\psi}_\delta$. Various applications of (3) can be found in electrical engineering and filter theory.

Consider a forcing in the form of uncorrelated random noise. For such a signal the spectrum S_τ is "white" or frequency independent, so that the mean-square response is

$$\overline{\psi^2} = \int_{-\infty}^{\infty} S_\psi d\omega = S_\tau \int_{-\infty}^{\infty} |\hat{\psi}_\delta|^2 d\omega, \tag{4}$$

where (3) has been used. Applying Parseval's theorem

$$\int_{-\infty}^{\infty} |\hat{\psi}_\delta|^2 d\omega = 2\pi \int_0^T \psi_\delta^2 dt,$$

Eq. (4) becomes

$$\overline{\psi^2} = 2\pi S_\tau \int_0^T \psi_\delta^2 dt. \tag{5}$$

The magnitude of the forcing spectrum S_τ depends on the sampling interval Δt. The frequency range of the spectrum is $(-\omega_N, \omega_N)$, where $\omega_N = \pi/\Delta t$ is the Nyquist frequency in rad s^{-1}. The mean-square forcing is then related to the spectrum by

$$\overline{\tau^2} = \int_{-\omega_N}^{\omega_N} S_\tau d\omega = 2\pi S_\tau/\Delta t.$$

Equation (5) then becomes

$$\overline{\psi^2} = \overline{\tau^2}\Delta t \int_0^T \psi_\delta^2 dt \tag{6}$$

which is valid if the forcing spectrum is white, and if Δt is small enough to resolve the natural period of the system.

In the absence of a decay, the impulse response $\psi_\delta(t)$ is a stationary series oscillating at the natural frequency of the system (the Coriolis frequency f in the present case). According to (6), the mean-square response in that case increases indefinitely with the increase of the record length T. On the other hand ψ_δ may be a decaying oscillatory series (having a decay scale t_d), which may be due to the presence of damping or an energy outflow to the surrounding points if ψ_δ is spatially dependent. The decay scale t_d defines a memory time, so that contributions due to earlier forcings are negligible in the superposition (1). The integral (6) also converges and $\overline{\psi^2}$ reaches a stationary value proportional to t_d. If t_d is large compared to the natural period, this stationary response can be quite large. A random forcing can then excite a large response at the natural frequency.

As a simple numerical illustration, consider the random wind forcing of a one-dimensional slab-like Ekman layer of thickness h. Assume a zero bottom stress, so that there is no viscous decay. The eastward velocity in this layer due to a northward impulsive forcing $\tau = \delta(t)$ can be easily shown to be

$$u_\delta = \frac{1}{h}\sin ft. \tag{7}$$

From (6) and (7), the mean-square eastward velocity due to a random forcing is

$$\overline{u^2} = \frac{\overline{\tau^2}\Delta t T}{2h^2}.$$

The rms velocity u' is therefore related to the rms forcing τ' by

$$\frac{u' f h}{\tau'} = \pi\left(\frac{2\Delta t}{t_i}\,\frac{T}{t_i}\right)^{1/2}, \tag{8}$$

where time has been expressed in terms of the inertial period $t_i = 2\pi/f$.

Equation (8) implies that the ensemble-averaged rms velocity for a record of length T varies as $T^{1/2}$. It is easy to show that the amplitude of the oscillations must then vary with the running time as $t^{1/2}$ on the average. Equation (8) also implies $u' \propto \Delta t\sqrt{N}$, where $N = T/\Delta t$ is the number of steps. This is similar to the result of a "random walk", in which the rms distance travelled in N uncorrelated steps of length Δr is $r' = \Delta r\sqrt{N}$. (See Feynman *et al.*, 1963, for a simple proof.) This similarity is no surprise, since both of these phenomena are the results of a random superposition of uncorrelated steps.

Equation (8) will now be tested against a numerical evaluation of the solution. For this, a random stress series is generated in the computer by setting the stress equal to a random number between (−0.5, 0.5), with equal probability of occurrence in this range. This produces a stress series with an rms value of $\tau' = (12)^{-1/2} = 0.2887$. The velocity field corresponding to such a random forcing at intervals of $\Delta t/t_i = 1/9$ is found from (1) and (7), and is shown in Fig. 1. The rms u' does seem to vary as $t^{1/2}$, as in (8). Testing with various Δt showed that u' also increased with Δt, in agreement with (8).

The rms velocity at the end of 30 cycles in Fig. 1 is found to be $u'fh/\tau' = 8.2$, which is in reasonable agreement with the value of $u'fh/\tau' = 8.1$ predicted from (8). In contrast recall that a step forcing generates a much smaller response of $u_{max}fh/\tau = 1$.

The energy relation is

$$\frac{1}{2}(u^2 + v^2) = \frac{1}{h}\int_0^t \tau v dt. \tag{9}$$

The right-hand side of (9) is plotted in the bottom panel of Fig. 1, and the agreement of the wind work and the resulting inertial energy is apparent. In agreement with (8), the work done (kinetic energy) is very closely proportional to t. Introduction of a decay time in the impulse response (7) showed that the work done and the resulting velocity field reach stationary states for $t > t_d$.

It may at first be surprising that a random τ and the resulting v should be correlated, as (9) implies. To see why they are correlated, note that the response can be viewed as a superposition of a series of random impulses at intervals of Δt. For simplicity assume that the impulses are of equal magnitude but random sign. An initial northward impulse immediately results in a northward velocity v_0. Because of the inertial rotation of the velocity vector, the northward velocity decreases to $v' < v_0$ after Δt at which time the second impulse is applied; the assumption $\Delta t \ll t_i$ will ensure that v' is also northward. The second impulse, which could be in either direction, will do positive work on

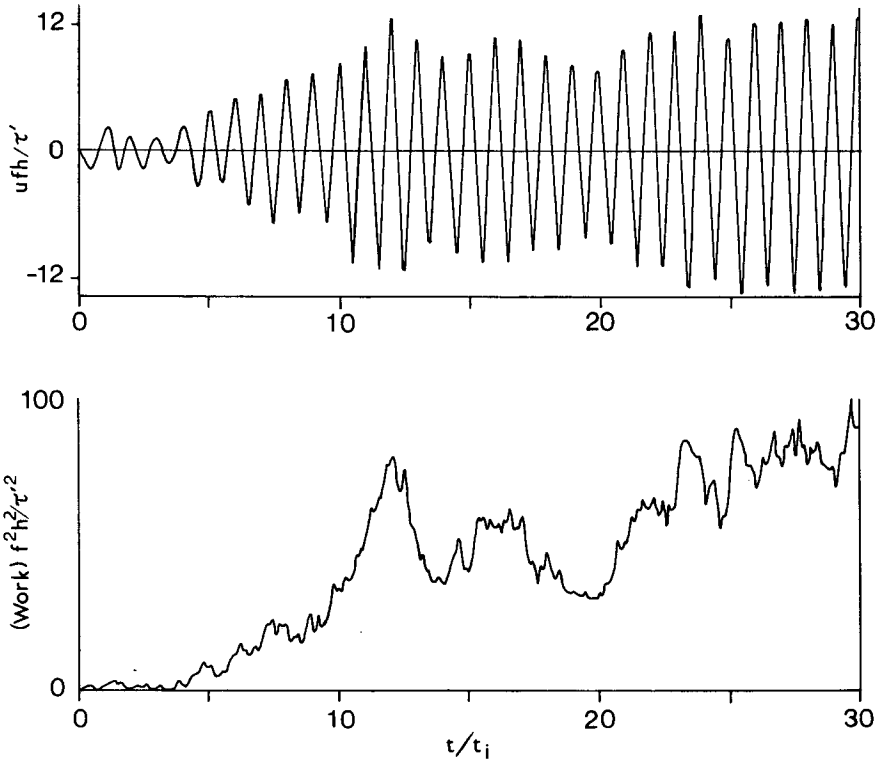

FIG. 1. Time series of u and surface-stress work in slab-like Ekman layer, forced by a purely random wind stress of rms value τ'. Note that the resulting amplitude far exceeds the step response, $u_{max}fh/\tau = 1$, and the close agreement between the surface work and kinetic energy.

the system if it is directed northward (since $v' > 0$). A southward second impulse, on the other hand, would result in a negative work, but its magnitude would be smaller than the positive work of the first impulse (since $v' < v_0$). Continuing this argument, the net work done after a series of impulses will be positive. Note that $v' \to v_0$ as $\Delta t \to 0$. The net work done, and the resultant velocities, would therefore go to zero as $\Delta t \to 0$, in agreement with (8).

Summarizing this section, it has been shown that large oscillations at the natural frequency can be built up by random forcing. The resulting amplitudes go like $t^{1/2}$ if there is no decay of the impulse response. If the impulse response decays in time t_d, the response to random forcing reaches stationary values proportional to $t_d^{1/2}$. These ideas will now be used to study the coastal inertial oscillations excited by a rapidly varying wind.

3. Results for step wind

Consider the coastal ocean on a flat shelf. The water depth is D, and the surface mixed-layer depth is h. The subsurface water has a buoyancy frequency $N(z)$, and a momentum and heat diffusivity ν. The coordinates (x, y, z) and velocity components (u, v, w) are taken in the east, north (alongshore), and upward directions, repectively. Pressure and density perturbations from a state of rest are p and ρ. The origin is placed at the surface–coast corner, with the ocean extending in the negative x-direction. The ocean bottom is assumed slippery. The alongshore independent model equations are

$$\left.\begin{aligned} &u_t - fv = -p_x + (\nu u_z)_z \\ &v_t + fu = (\nu v_z)_z \\ &0 = -p_z - g\rho \\ &u_x + w_z = 0 \\ &\rho_t - \frac{N^2}{g} w = (\nu\rho)_{zz} \end{aligned}\right\}. \tag{9}$$

Solutions are obtained by decomposing the variables in terms of vertical normal modes:

$$\left.\begin{aligned} u, v, p &= \sum_{n=0}^{\infty} (u_n, v_n, p_n)\phi_n \\ w &= \sum_{n=0}^{\infty} w_n \int_{-D}^{z} \phi_n dz \\ \rho &= \sum_{n=0}^{\infty} \rho_n \phi_{nz} \end{aligned}\right\}. \tag{10}$$

For $n > 1$, the vertical modes are given by

$$c_n^2 \left(\frac{\phi_{nz}}{N^2}\right)_z + \phi_n = 0, \quad \phi_{nz} = 0 \quad \text{at} \quad z = 0, -D, \tag{11}$$

where the eigenvalues c_n are the long internal wave speeds. The expansion coefficients satisfy

$$\left.\begin{aligned} &(\partial_t + \nu_n)u_n - fv_n + p_{nx} = \tau_n^x \\ &(\partial_t + \nu_n)v_n + fu_n = \tau_n^y \\ &(\partial_t + \nu_n)p_n + c_n^2 u_{nx} = 0 \\ &c_n^2 w_n = (\partial_t + \nu_n)p_n \\ &\rho_n = -p_n/g \end{aligned}\right\}. \tag{12}$$

Here $\nu_n = \nu N^2/c_n^2$ is the viscous damping coefficient. The coupling coefficients of each mode to the wind stress $\tau = [\tau^x, \tau^y]$ are

$$\tau_n^x = \tau^x \Big/ \int_{-D}^{0} \phi_n^2 dz, \quad \tau_n^y = \tau^y \Big/ \int_{-D}^{0} \phi_n^2\, dz. \tag{13}$$

Solutions for a step-input alongshore wind $\tau^y H(t)$, where $H(t)$ is the Heaviside function, are given in KCM. Solutions for a cross-shelf step-input wind can be found in a similar way. The complete response to the step input $\tau = [\tau^x H(t), \tau^y H(t)]$ is

$$P_{nH} = H\left(t + \frac{x}{c_n}\right) c_n \tau_n^x \{1\} * \{e^{-\nu_n t} J_0(f^2 t^2 - x_n^2)^{1/2}\} + H\left(t + \frac{x}{c_n}\right) f c_n \tau_n^y \left\{\frac{1 - e^{-\nu_n t}}{\nu_n}\right\} * \left\{e^{-\nu_n t} J_0(f^2 t^2 - x_n^2)^{1/2}\right\},$$

$$u_{nH} = \frac{\tau_n^x}{\nu_n^2 + f^2}\left[\nu_n - e^{-\nu_n t}(\nu_n \cos ft - f \sin ft)\right] + \frac{\tau_n^y}{\nu_n^2 + f^2}\left[f - e^{-\nu_n t}(\nu_n \sin ft + f \cos ft)\right] - \frac{H(t + x/c_n)\tau_n^x e^{-\nu_n t}}{\nu_n^2 + f^2}$$

$$\times \left[\nu_n e^{\nu_n (t + x/c_n)} - \nu_n \cos(ft + x_n) + f \sin(ft + x_n)\right] - \frac{H(t + x/c_n)\tau_n^y e^{-\nu_n t}}{\nu_n^2 + f^2}\left[f e^{\nu_n (t + x/c_n)} - \nu_n \sin(ft + x_n)\right.$$

$$\left. - f \cos(ft + x_n)\right] + \frac{H(t + x/c_n)\tau_n^x f x_n}{\nu_n^2 + f^2}\{\nu_n - e^{-\nu_n t}(\nu_n \cos ft - f \sin ft)\} * \left\{\frac{e^{-\nu_n t} J_1(f^2 t^2 - x_n^2)^{1/2}}{(f^2 t^2 - x_n^2)^{1/2}}\right\}$$

$$- \frac{H(t + x/c_n)\tau_n^y f x_n}{\nu_n^2 + f^2}\{f - e^{-\nu_n t}(\nu_n \sin ft + f \cos ft\} * \left\{\frac{e^{-\nu_n t} J_1(f^2 t^2 - x_n^2)^{1/2}}{(f^2 t^2 - x_n^2)^{1/2}}\right\}.$$

$$v_{nH} = -\frac{\tau_n^x}{\nu_n^2+f^2}[f - e^{-\nu_n t}(\nu_n \sin ft + f\cos ft)] + \frac{\tau_n^y}{\nu_n^2+f^2}[\nu_n + e^{-\nu_n t}(f\sin ft - \nu_n \cos ft)] + \frac{H(t+x/c_n)\tau_n^x e^{-\nu_n t}}{\nu_n^2+f^2}$$

$$\times [fe^{\nu_n(t+x/c_n)} - \nu_n \sin(ft+x_n) - ft\cos(f+x_n)] - \frac{H(t+x/c_n)\tau_n^y e^{-\nu_n t}}{\nu_n^2+f^2}\left[f\sin(ft+x_n) - \nu_n\cos(ft+x_n)\right.$$

$$\left. + \nu_n + \frac{f^2}{\nu_n}[1 - e^{\nu_n(t+x/c_n)}]\right] + \frac{H(t+x/c_n)\tau_n^x f x_n}{\nu_n^2+f^2}\{f - e^{-\nu_n t}(\nu_n \sin ft + f\cos ft)\} * \left\{\frac{e^{-\nu_n t}J_1(f^2t^2 - x_n^2)^{1/2}}{(f^2t^2+x_n^2)^{1/2}}\right\}$$

$$- \frac{H(t+x/c_n)\tau_n^y f x_n}{\nu_n^2+f^2}\left\{e^{-\nu_n t}\left(f\sin ft - \nu_n\cos ft + \nu_n + \frac{f^2}{\nu_n}\right) - \frac{f^2}{\nu_n}\right\} * \left\{\frac{e^{-\nu_n t}J_1(f^2t^2 - x_n^2)^{1/2}}{(f^2t^2 - x_n^2)^{1/2}}\right\}. \quad (14)$$

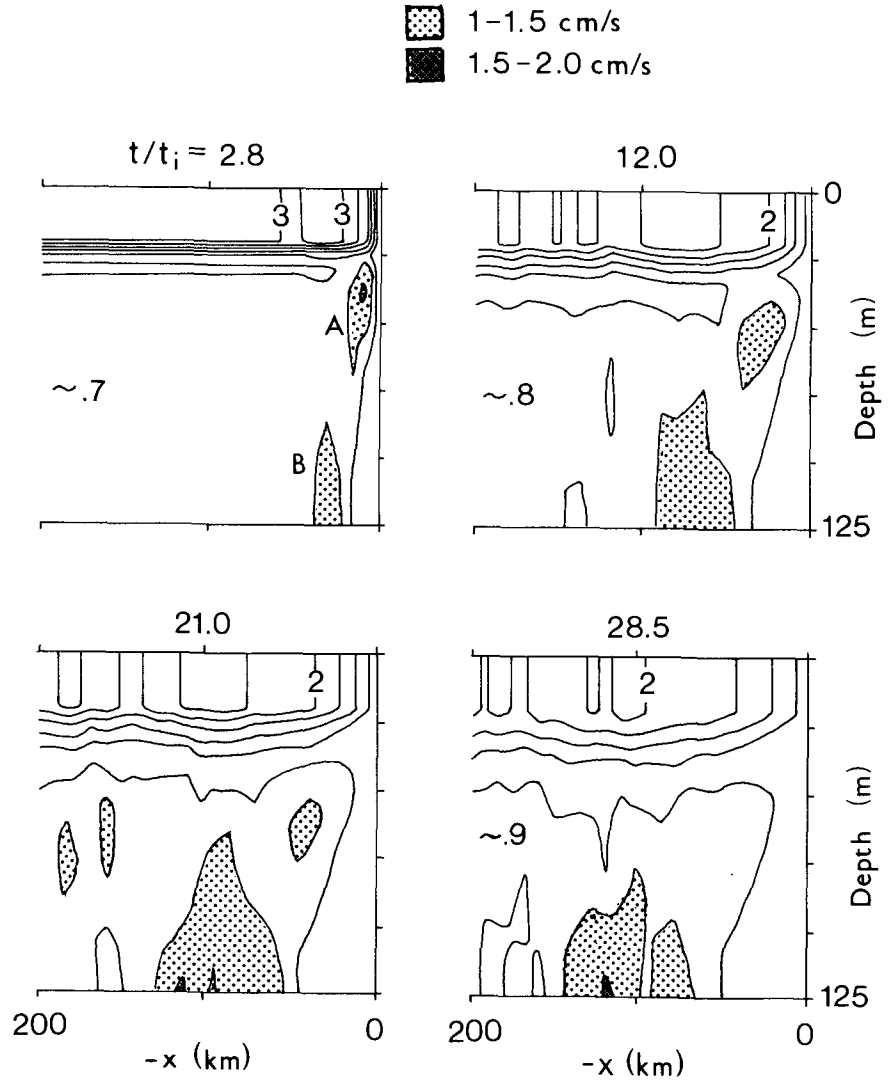

FIG. 2. Contour plots of inertial amplitude for various times. Forcing is a step-input alongshore wind. Contour interval is 0.5 cm s^{-1}. Subsurface regions with amplitudes above 1.0 cm s^{-1} are shaded. Small regions of amplitude larger than 1.5 cm s^{-1} are shaded heavily; these occur within region A at $t/t_i = 2.8$ and near the bottom at $t/t_i = 21.0$ and 28.5. Amplitude in regions of nearly uniform value is indicated by ~ amplitude.

Here $x_n = xf/c_n$, J_0 and J_1 are the Bessel functions, and the asterisk represents the convolution product of two functions delineated by braces, with the integral going from $-x/c_n$ to t. For example

$$\{f(t)\}*\{g(t)\} = \int_{-x/c_n}^{t} f(t-\alpha)g(\alpha)d\alpha.$$

In (14) the subscript H on p_n, u_n and v_n is used as a reminder that these are the step responses. Note the v_{nH} due to τ^x is equal and opposite to u_{nH} due to τ^y. The solutions satisfy the zero initial conditions, and the following boundary conditions: $u = 0$ at $x = 0$; (u, v, p) are bounded as $-x \to \infty$; and $u_z = v_z = w = 0$ at $z = 0, -D$. They contain the nonoscillatory component of the response, as well as the inertio-gravity waves which are of interest here. Terms not multiplied by $H(t + x/c_n)$ are the unbounded solutions and those multiplied by $H(t + x/c_n)$ are the waves generated by the presence of the coast. A detailed discussion of these equations without the τ^x terms is given in KCM.

Step-input calculations up to 5 days are discussed extensively in KCM. A similar calculation up to 25 days will be briefly discussed here, bringing out some new information. The parameters used here are

$\tau = 1$ dyn cm^{-2}
$N = 10^{-2}$ s^{-1}
$f = 10^{-4}$ s^{-1} (inertial period $t_i = 17.45$ h)
$h = 20$ m
$D = 125$ m
$\nu = 1$ cm^2 s^{-1}.

The values of D and ν chosen here are smaller than those in the KCM calculations.

Profiles of the first 50 baroclinic modes are determined by solving the eigenvalue problem (11). The barotropic mode is taken to be $\phi_0(z) = 1$ and $c_0 = (gD)^{1/2}$. Solutions are found from (14) and (10) for unit step inputs of τ^x and τ^y by summing over 51 normal modes, in which the solutions converged. A complete calculation up to 25 days took over one hour of computing time on the CRAY-1 computer.

Only the results for $\tau^y = 1$ dyn cm^{-2} will be presented in this section, since those for $\tau^x = 1$ dyn cm^{-2} are essentially similar in nature. The near-inertial oscillations are extracted from the solution by complex demodulation of the time series at inertial frequency. [They were determined in KCM by a different method, with practically the same result.] Only these demodulated "inertial" series will be presented, except in Fig. 6 where the entire solution is considered.

Figure 2 shows the contour plots of the inertial amplitude for various times, in which the following characteristics should be noticed:

1) The amplitude adjacent to the coast decays monotonically throughout the water column (coastal inhibition).

2) The loss of energy in the surface layer is caused by a downward flux from the corner. This results in a region of gain A in which the maximum amplitude of 1.5 cm s^{-1} is reached at $t/t_i \approx 3$.

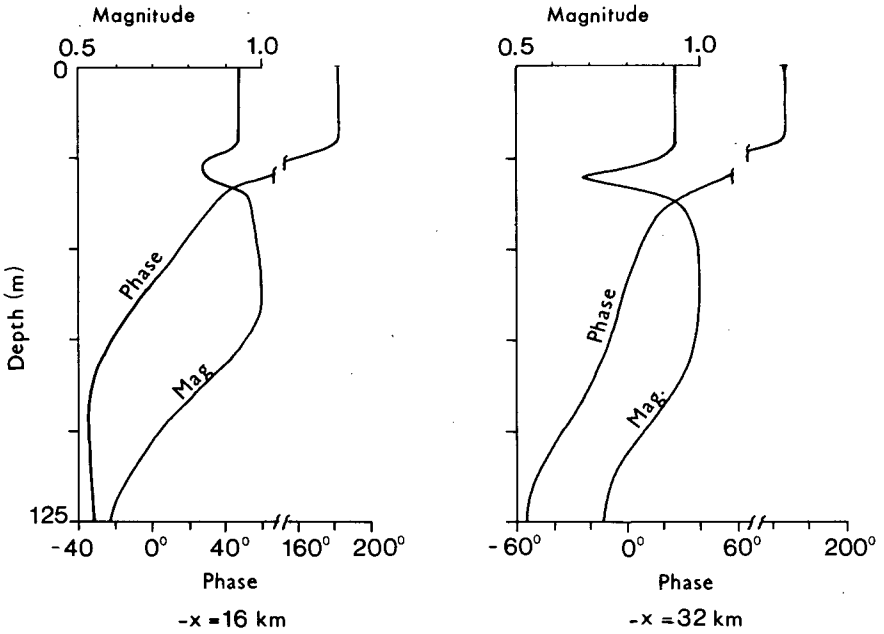

FIG. 3. Vertical correlation of velocity vectors. Forcing is a step-input alongshore wind. Left and right panels refer to offshore distances of 16 and 32 km, respectively. All correlations are computed with respect to 60 m depth. A positive ∂(phase)/∂z signifies upward phase speed. Note the generally upward phase propagation, except below 90 m depth at $-x = 16$ km.

3) Another region of gain B moves offshore and upward near the bottom. This region is apparently created by a combination of the bottom reflection of some of the downward flux from the surface layer, and the loss of near-shore energy near the bottom.

4) There is a general decay in the surface layer throughout the 32 cycles of computation, with the amplitudes decreasing from 4 cm s^{-1} to about 2 cm s^{-1}.

5) In contrast, most of the subsurface region preserves its original amplitude of 0.7 cm s^{-1}, although the region of gain A decays.

It should be noted here that the amplitude evolution of the impulse response $u_\delta(\mathbf{x}, t) \equiv \partial u_H/\partial t$ is very similar to that in Fig. 2, since u_H is an almost periodic series.

Phase differences in the flow field can best be described by the complex correlation coefficient of velocity vectors (Kundu 1976a), defined as the normalized form of the inner product

$$R = \overline{w\dagger(\mathbf{x}, t)w(\mathbf{x}_0, t)},$$

where $w = u + iv$. The magnitude of R gives a *weighted* average correlation, and the phase angle of R gives the average anticlockwise angle of vector at $\mathbf{x}$ with respect to the vector at $\mathbf{x}_0$. Figure 3 shows the magnitude and phase of vertical correlation at two offshore locations. The phase propagation is generally upward, except near the bottom close to the coast

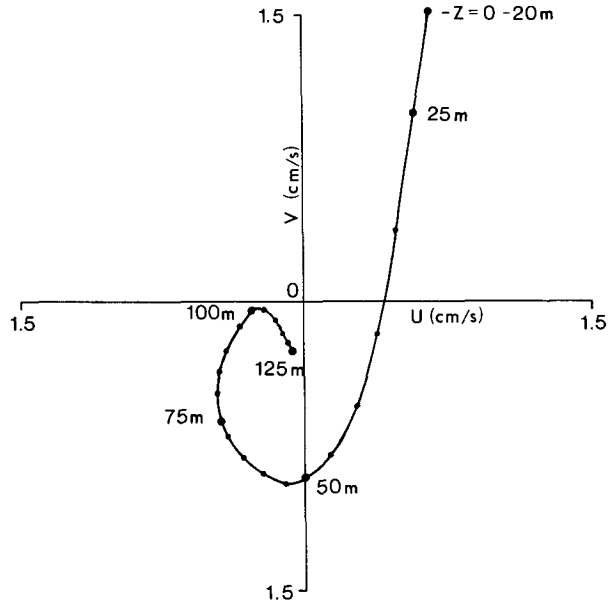

FIG. 4. Vertical distribution of velocity vectors at $t/t_i = 19$ and $-x = 32$ km. Forcing is a step-input alongshore wind. Each point corresponds to the instantaneous current at a certain depth. Larger dots are separated by 25 m and smaller dots by 5 m. Each current vector is rotating clockwise at a near-inertial frequency, so that the current at 100 m depth leads those above and below. Phase speed below 100 m is therefore downward, implying bottom reflection.

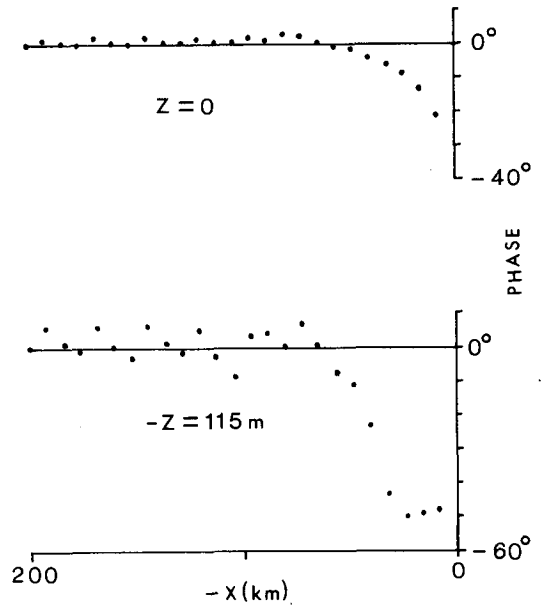

FIG. 5. Phase angle of horizontal correlation of velocity vectors. Forcing is a step-input alongshore wind. Upper and lower panels refer to the surface and 115 m depth, respectively. Phases are computed with respect to the vector at $-x = 200$ km. Negative phase angle signifies that nearshore currents lead.

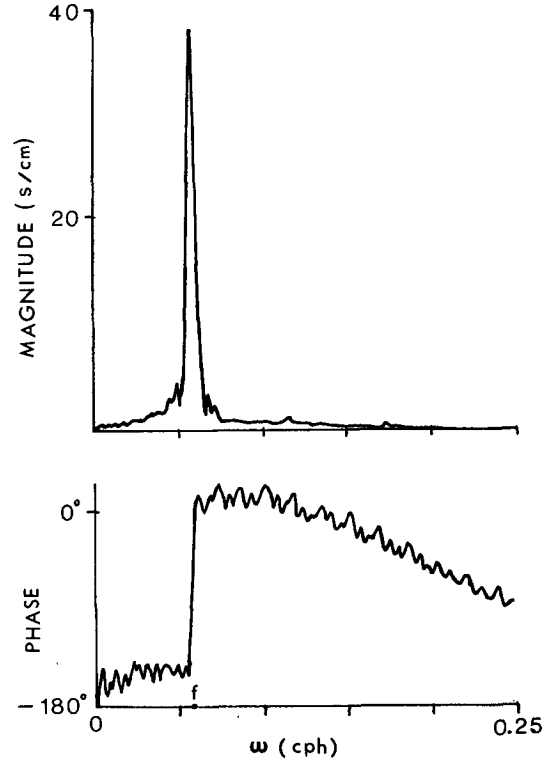

FIG. 6. Magnitude and phase angle of transfer function $\hat{u}_\delta(\omega)$ of cross-shelf current at $(-x, -z) = (72$ km, 45 m) due to alongshore wind. Note the nearly 180° phase shift across the resonant frequency $\omega = f$.

($-x$ = 16 km) where it is downward, implying bottom reflection. At later times bottom reflection takes place farther offshore. This is evident in the hodograph plot (Fig. 4), showing bottom reflection below 100 m at an offshore distance of 32 km.

The horizontal phase differences at two depths are shown in Fig. 5. The values fall on a smooth line at the surface where the correlation is high, but not at the deeper layer where the correlation is lower. Offshore of 100 km the vectors are oriented practically in the same direction. The nearshore vectors lead, signifying an offshore phase propagation. A typical nearshore horizontal wavelength is $\lambda_H = 2\pi[\partial(\text{phase})/\partial x]^{-1} \sim 400$ km, far larger than the 70 km wavelength suggested in KCM essentially based on the dispersion relation. It is apparently inappropriate to apply the dispersion relation $m = k/(\omega^2 - f^2)^{1/2}$ for inertio-gravity waves and use local values of the parameters, because the WKB approximation is not valid in a situation where only a small part of a complete wave is present in the flow field. (Note that the total phase variation in Fig. 5 is only 50°.)

The magnitude and phase of the transfer function $\hat{u}_\delta$ at a point is shown in Fig. 6. It is found by Fourier transforming the step response u_H and multiplying by $i\omega$. The transfer function peaks near $\omega = f$, with its phase changing by nearly 180° across the resonant frequency. This characteristic is similar to that of other linear oscillatory systems (for example, see Fig. 2.5 of Bendat and Piersol, 1971). The −180° phase of the response near $\omega = 0$ is consistent with the fact that a northward alongshore wind generates a negative steady u below the surface layer.

4. Results for time-varying wind

In this section the coastal response due to a time-varying wind will be constructed by superposing the

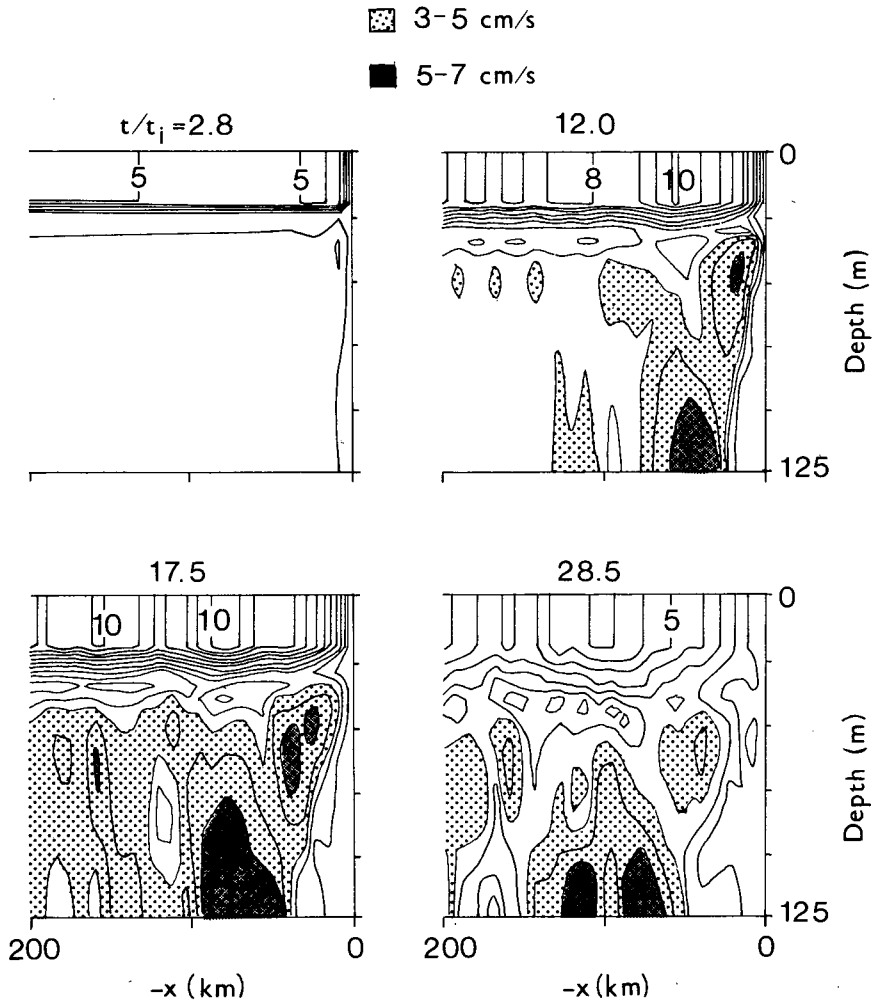

FIG. 7. Contour plots of inertial amplitude for various times. Forcing is a random alongshore wind between (−0.5, 0.5) dyn cm^{-2}. Contour interval is 1.0 cm s^{-1}. Subsurface regions with amplitude above 3 cm s^{-1} are shaded.

step input solutions of the last section. Two types of forcing will be considered, namely the completely random wind and an observed wind.

Consider first the case of a random alongshore wind in the range (−0.5, 0.5) dyn cm^{-2}, having a uniform probability in this range. The stress has a zero mean and an rms value of $\tau' = 0.2887$ dyn cm^{-2}. The corresponding eastward velocity is found from a discrete version of (1), namely

$$u(\mathbf{x}, t) = \sum_{m=0}^{M} \Delta\tau^y(m\Delta t) u_H^y(\mathbf{x}, t - m\Delta t),$$

where $t = M\Delta t$, $\Delta\tau^y$ is the stress change at time $m\Delta t$, and u_H^y the response due to a unit step input of τ^y. The sampling interval is chosen to be $\Delta t = 2$ h.

The resulting amplitude evolution (Fig. 7) shows maximum surface values of 11 cm s^{-1} and maximum subsurface values of 6–7 cm s^{-1}. These are several times larger than those due to a step input of 1 dyn cm^{-2} (Fig. 2), a fact already noted in a simpler situation without horizontal variability (Fig. 1). Note in Fig. 7 that the continuous superposition has generally energized the subsurface water more than the surface water. This is consistent with (6), and the fact that the impulse response (whose amplitude evolution is similar to Fig. 2) monotonically decays in the surface layer but not below, except very close to the coastal wall. Physically, the effect is due to the continuous downward flux of energy from the surface–coast corner. The persistence time (Fig. 8) of the velocity is about 10–15 cycles.

The vertical correlation (Fig. 9) is less than that due to step forcing (Fig. 3), and again shows the nearly 180° phase change just below the mixed layer and the bottom reflection near the coast.

The coastal system is next forced with an observed wind stress series. The data chosen for this (Fig. 10) are wind measurements off the coast of Oregon during the summer of 1973 (Halpern *et al.*, 1974). The alongshore stress during the period of calculation has a mean of −0.58 dyn cm^{-2}, a standard deviation of 0.71 dyn cm^{-2}, and a peak value on July 12 of −3.6 dyn cm^{-2}. The cross-shelf stress is small with a standard deviation of 0.04 dyn cm^{-2}.

The flow is computed by summing contributions from both components of the wind. The eastward velocity, for example, is found from

$$u(\mathbf{x}, t) = \sum_{m=0}^{M} \Delta\tau^x(m\Delta t) u_H^x(\mathbf{x}, t - m\Delta t) + \sum_{m=0}^{M} \Delta\tau^y(m\Delta t) u_H^y(\mathbf{x}, t - m\Delta t),$$

where the unit step responses u_H^x and u_H^y are found from the analytical expressions (14). The sampling interval $\Delta t = 2$ h.

The resulting amplitude plot (Fig. 11) shows surface values of 10–17 cm s^{-1} and subsurface values of 3–9

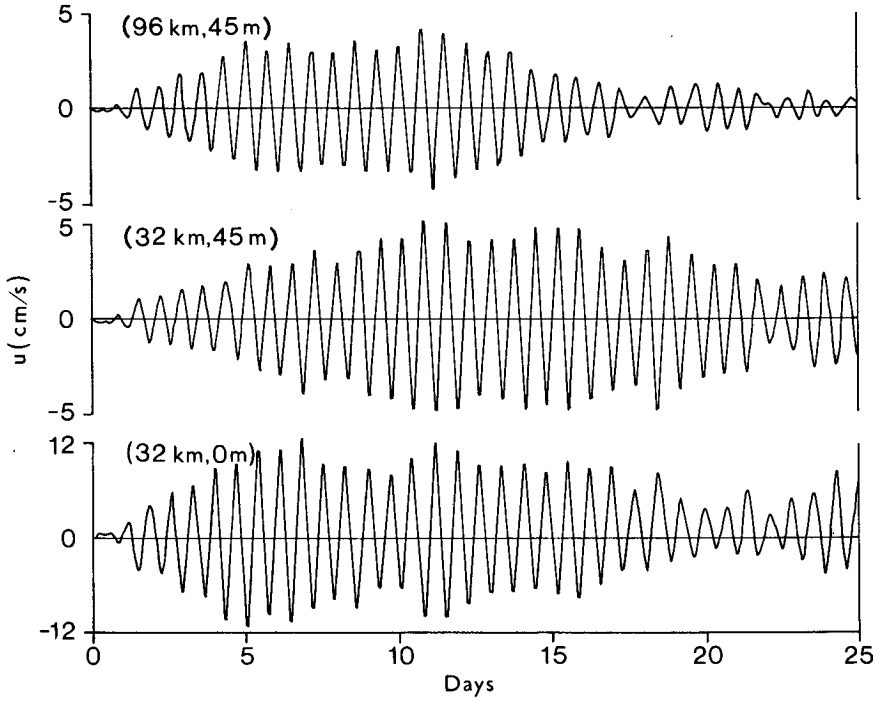

FIG. 8. Time series of u at three locations indicated in parentheses. Forcing is a random alongshore wind between (−0.5, 0.5) dyn cm^{-2}.

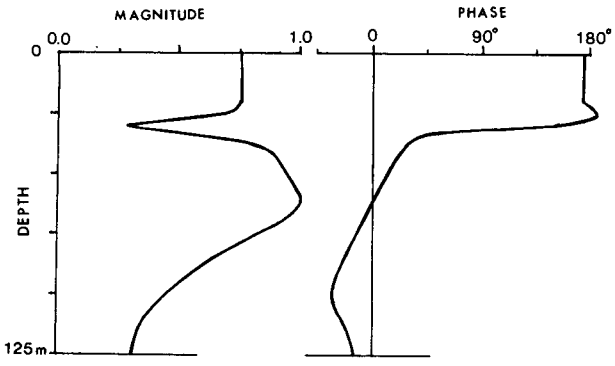

FIG. 9. Vertical correlation of velocity vectors at an offshore distance of 16 km. Forcing is a random alongshore wind between $(-0.5, 0.5)$ dyn cm^{-2}. The correlation is computed with respect to the 60 m depth. Note the generally upward phase propagation, except below 105 m depth. Also note that the correlation magnitude is lower than that for a step forcing shown in Fig. 3.

cm s^{-1}. A time-series plot (Fig. 12) shows that the persistence time is typically 10–15 cycles. Vertical correlation was found to have magnitudes similar to that shown in Fig. 9. The persistence time and correlation scale are therefore larger than those observed.

5. Summary and remarks

The excitation of coastal inertial oscillations by a rapidly varying wind has been investigated. It has been shown that the mean-square response to a *completely random* forcing is

$$\overline{\psi^2} = \overline{\tau^2}\Delta t \int_0^T \psi_\delta^2 dt, \tag{6}$$

where $\overline{\tau^2}$ is the mean-square wind stress, Δt the sampling interval, T the record length and ψ_δ is the impulse response. An undamped one-dimensional system forced by random noise therefore oscillates at the natural frequency of the system, with the rms amplitude increasing as $t^{1/2}$. The $t^{1/2}$ increase of the rms response is similar to that in a random walk, and results from a superposition of uncorrelated steps. In a system in which ψ_δ is a decaying series, the rms response initially increases with time as $t^{1/2}$ and reaches stationarity in the decay scale for ψ_δ. Continuous random forcing therefore preferentially increases the subsurface amplitudes since the energy flux from the surface–coast corner causes a surface decay and a subsurface growth of ψ_δ.

The coastal model used is that of Kundu *et al.* (1983), which was forced with a step-input constant, alongshore wind. It is linear, alongshore-independent, vertically diffusive and stratified. The parameters assumed here are $D = 125$ m, $h = 20$ m, $\nu = 1$ cm^2 s^{-1}, $f = 10^{-4}$ s^{-1} and $N = 10^{-2}$ s^{-1}. A step forcing of 1 dyn cm^{-2} generates an inertial oscillation of 4 cm s^{-1} in the surface layer. It undergoes rapid decay near the coast, forcing a downward flux of inertial energy from the surface–coast corner. The subsurface oscillations are 0.7–1.5 cm s^{-1}. They are highly coherent in depth and not intermittent in time.

Application of a completely uncorrelated random alongshore wind in the range $(-0.5, 0.5)$ dyn cm^{-2}, having a standard deviation of 0.29 dyn cm^{-2}, in-

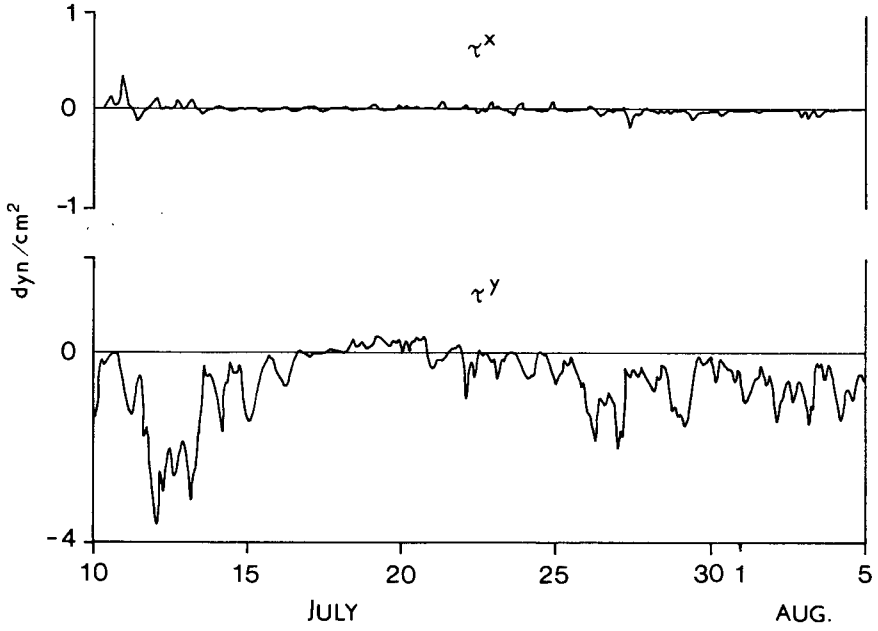

FIG. 10. Observed wind stress components off the coast of Oregon during 1973. Note the different scales for τ^x and τ^y.

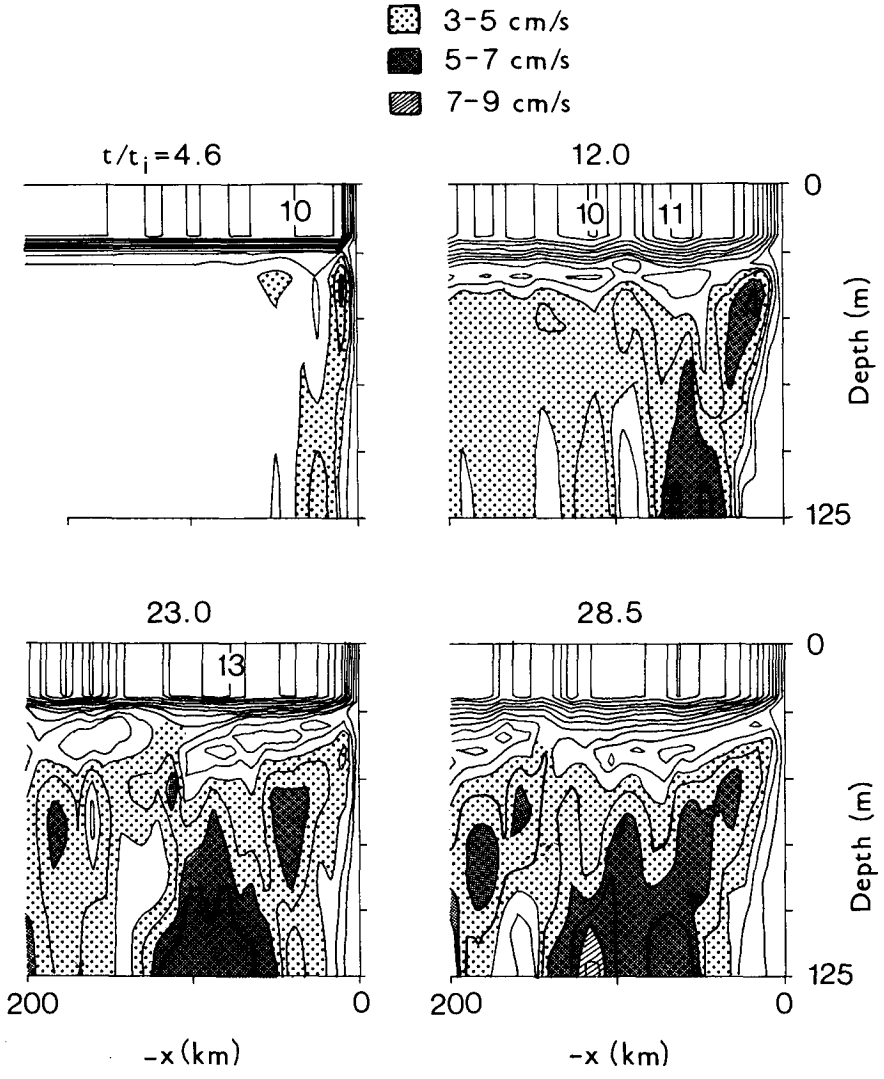

FIG. 11. Contour plots of inertial amplitude for various times. Forcing is the observed wind of Fig. 10. Contour interval is 1.0 cm s^{-1}. Subsurface regions with amplitude above 3 cm s^{-1} are shaded.

creases the inertial amplitudes everywhere. They are typically 8–11 cm s^{-1} in the surface layer and 3–7 cm s^{-1} below. The model is also forced by an observed wind stress series having a peak value of 3.6 dyn cm^{-2} and a standard deviation of 0.7 dyn cm^{-2}. The resulting surface and subsurface oscillations are 10–17 and 3–9 cm s^{-1}, respectively. Compared to the step forcing, the inertial oscillations generated by these time varying forcings are less coherent in the vertical, and more intermittent in time (typically persistent for 10–15 cycles).

The predicted sharp reversal of phase at the mixed layer bottom does not agree with observations off Oregon (Kundu 1976b). This is probably due to the absence of a well defined mixed layer (in which the wind force can be assumed uniformly distributed) in the region of observation. However, the phase reversal does agree with the Mediterranean observations of Millot and Crépon (1981), in which the water column had a well defined upper mixed layer.

The bottom trapping of energy in the model is a consequence of the slip condition $u_z = v_z = 0$ used, which necessarily generates a local extremum of velocity. A no-slip bottom condition would avoid this, but energetic inertial oscillations just above the bottom Ekman layer would still exist, as seen in the finite-difference calculations of Kundu (1984). Bottom intensification of inertial energy is also seen in the calculations of Gill (1984) and the observations of Saunders (1983).

The mechanism of coastal inhibition, which leads to the downward propagation of inertial energy from

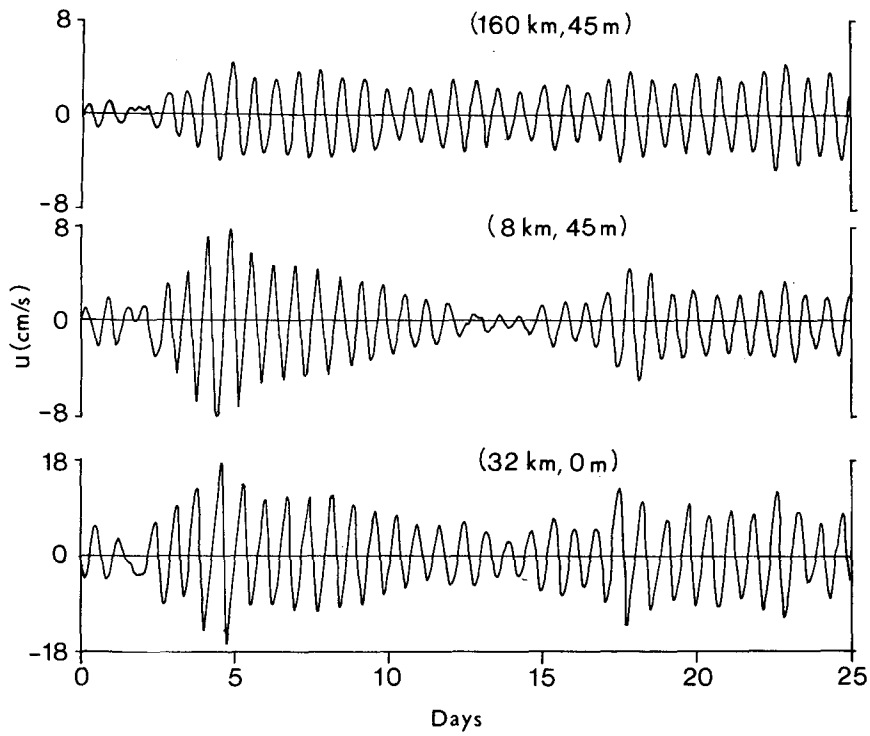

FIG. 12. Time series of u at three locations indicated in parentheses. Forcing is the observed wind of Fig. 10.

the surface–coast corner, strictly needs a vertical coast. It is therefore necessary to speculate on what would happen over a realistic nearshore bottom topography. The model group velocity from the coast–surface corner makes an angle of 0.2° with the horizontal (Fig. 2), which is of the order of typical topographic slopes. Flow over a steeper topography would behave essentially according to the model, but that over a gentler bottom slope could be different. However, the coastal inhibition would still act to force the inertial energy out of the corner, perhaps in a modified way; the problem needs a numerical study. Moreover, it is possible that beach processes in fact simulate a near-vertical "wall" to the offshore flow in the top 20 m or so. In that case the corner flux would simply undergo several reflections between the gently sloping bottom and the ocean surface as it carries energy offshore; the dynamics would otherwise be essentially unchanged.

The model results should be judged against coastal observations, which show subsurface oscillations as large as 10–15 cm s^{-1}, low vertical coherence scales (~20 m), and high intermittency (persistence time ~ 5–20 cycles). The effect of rapidly varying the wind stress has therefore greatly improved the model results over those due to a step input, but not completely removed the discrepancy with observations. A spatially varying wind stress may be able to improve the model results further, because of additional downward fluxes of energy from regions of sharp change in the wind stress. Mechanisms neglected here, for example, the resonantly interacting internal wave triads (McComas and Bretherton, 1977), might also be important in the real ocean.

It is intriguing to speculate whether the superposition mechanism proposed here can help explain some of the subsurface oscillations observed in the open ocean. Calculations of Pollard (1970) and Gill (1984) show that the subsurface step response in the open ocean is much smaller than the observed amplitudes. As a result, it is generally agreed that the deep-ocean inertial oscillations are not wind forced, but forced by bottom roughness or are due to the poleward propagation of higher-frequency internal waves to their turning latitudes (Fu, 1981). However, the impulse response in the deep ocean persists for many months (Gill, 1984), and therefore the wind forcing over a long enough time cannot be completely ruled out.

Acknowledgments. The work was supported by the National Science Foundation under Grant OCE-83-08148. Computing time on the GRAY-1 was donated by the National Center for Atmospheric Research, Boulder, Colorado. I thank J. Price for comments on the manuscript, and Kevin Kohler for help with the programming.

REFERENCES

Bendat, J. S., and A. G. Piersol, 1971: *Random Data: Analysis and Measurement Procedures.* Wiley-Interscience, 407 pp.

Denbo, D. W., and J. S. Allen, 1984: Rotary empirical orthogonal function analysis of currents near the Oregon coast. *J. Phys. Oceanogr.*, **14,** 35–46.

Feynman, R. P., R. B. Leighton and M. Sands, 1963: *The Feynman Lectures on Physics, Vol. I.* Addison-Wesley.

Fu, L. L., 1981: Observations and models of inertial waves in the deep ocean. *Rev. Geophys. Space Phys.*, **19,** 141–170.

Gill, A. E., 1984: On the behaviour of internal waves in the wakes of storms. *J. Phys. Oceanogr.*, **14,** 1129–1151.

Halpern, D., J. R. Holbrook and R. M. Reynolds, 1974: A compilation of wind, current and temperature measurements: Oregon, July and August 1973. CUEA Tech. Rep. 6, Ref. M74–73. Dept. of Oceanogr., University of Washington, 190 pp.

Hamilton, P., 1984: Topographic and inertial waves on the continental rise of the Mid-Atlantic Bight. *J. Geophys. Res.*, **89,** 695–710.

Kundu, P. K., 1976a: Ekman veering observed near the ocean bottom. *J. Phys. Oceanogr.*, **6,** 238–242.

——, 1976b: An analysis of inertial oscillations observed near Oregon coast. *J. Phys. Oceanogr.*, **6,** 879–893.

——, 1984: Numerical calculations of coastal flow with turbulent dynamics. *Deep-Sea Res.*, **31,** 39–60.

——, S-Y. Chao and J. P. McCreary, 1983: Transient coastal currents and inertio-gravity waves. *Deep-Sea Res.*, **30,** 1059–1082.

McComas, C. H., and F. P. Bretherton, 1977: Resonant interactions of oceanic internal waves. *J. Geophys. Res.*, **82,** 1397–1412.

Millot, C., and M. Crépon, 1981: Inertial oscillations on the continental shelf of the Gulf of Lions—observations and theory. *J. Phys. Oceanogr.*, **11,** 639–657.

Pollard, R. T., 1970: On the generation by winds of inertial oscillations in the ocean. *Deep-Sea Res.*, **17,** 795–812.

——, and R. C. Millard, 1970: Comparison between observed and simulated wind-generated inertial oscillations. *Deep-Sea Res.*, **17,** 813–821.

Price, J. F., 1983: Internal wave wake of a moving storm. Part I: Scales, energy budget and observations. *J. Phys. Oceanogr.*, **13,** 949–965.

Saunders, P. M., 1983: Benthic observations on the Madeira Abyssal Plain: Currents and dispersion. *J. Phys. Oceanogr.*, **13,** 1416–1429.

Thomson, R. E., and W. S. Huggett, 1981: Wind-driven inertial oscillations of large spatial coherence. *Atmos.-Ocean,* **19,** 281–306.